Journal of Solid State Chemistry 184 (2011) 2412–2419

Contents lists available at ScienceDirect

Journal of Solid State Chemistry

journal homepage: www.elsevier.com/locate/jssc

Structural originations of irreversible capacity loss from highly lithiated copper oxides

Corey T. Love [a,*], Wojtek Dmowski [b], Michelle D. Johannes [a], Karen E. Swider-Lyons [a]

[a] U.S. Naval Research Laboratory, Washington, DC 20375-5342, USA
[b] University of Tennessee, 1512 Middle Drive, Knoxville, TN 37996, USA

ARTICLE INFO

Article history:
Received 5 April 2011
Received in revised form
1 July 2011
Accepted 6 July 2011
Available online 19 July 2011

Keywords:
Lithium-ion battery
Cathode
Li_2CuO_2
Capacity loss
Pair-distribution function

ABSTRACT

We use electrochemistry, high-energy X-ray diffraction (XRD) with pair-distribution function analysis (PDF), and density functional theory (DFT) to study the instabilities of Li_2CuO_2 at varying state of charge. Rietveld refinement of XRD patterns revealed phase evolution from pure Li_2CuO_2 body-centered orthorhombic (*Immm*) space group to multiphase compositions after cycling. The PDF showed CuO_4 square chains with varying packing during electrochemical cycling. Peaks in the $G(r)$ at the Cu–O distance for delithiated, $LiCuO_2$, showed CuO_4 square chains with reduced ionic radius for Cu in the 3+ state. At full depth of discharge to 1.5 V, CuO was observed in fractions greater than the initial impurity level which strongly affects the reversibility of the lithiation reactions contributing to capacity loss. DFT calculations showed electron removal from Cu and O during delithiation of Li_2CuO_2.

Published by Elsevier Inc.

1. Introduction

Charge storage in secondary lithium-ion battery (LIB) cathode materials is a critical technology to the development of high-energy power sources for electric and hybrid vehicles; however there are relatively few practical materials. The range of commercially viable cathode compositions for LIBs must be broadened to market cost-competitive electric drive vehicles. To meet future performance requirements, cathodes must have high lithium capacity over thousands of charge and discharge cycles while being safe, inexpensive, and environmentally benign with the ability to be recycled. Lithiated copper oxides offer many environmental and cost-savings benefits over cobalt-based chemistries. Copper is an abundant relatively inexpensive transition metal with lower toxicity than cobalt and nickel [1]; however the over-lithiated copper oxides, Li_2CuO_2 and $Li_3Cu_2O_4$, are limited by poor capacity retention after a high initial charge cycle [1–4]. High initial charge capacity of Li_2CuO_2 is based upon an orthorhombic body-centered, *Immm*, structure which provides a large number of lithium sites [5]. Li_2CuO_2 can theoretically de-intercalate up to 2.0 Li^+ per unit formula, which far exceeds the practical limit of lithium ions intercalated per unit formula by commercial battery materials, 0.5 Li^+ for $LiCoO_2$ and 1.0 Li^+ for $LiFePO_4$. Poor capacity retention during the lithium extraction reaction limits the application of Li_2CuO_2 as active cathode materials, however Li_2CuO_2 has been successfully explored as a sacrificial additive to allow stable anode solid electrolyte interface (SEI) formation during an initial cycle at high states of charge [4].

While theoretical evaluation of Li_2CuO_2 indicates a high Li^+ capacity, its practical evaluation shows that the high specific capacity is only achieved upon the initial charge [6,7]. Several authors have commented on structural distortions associated with the lithiation and de-lithiation of Li_2CuO_2 [2–4]. The loss of capacity has been attributed to both structural transformations and chemical side reactions where the larger orthorhombic structure collapses into a denser-packed layered structure during delithiation [6]. First principles computational efforts were not able to identify a suitable 4-fold coordination transition metal (Cu, Pt, Fe) to stabilize iso-structural Li_2NiO_2 in the *Immm* structure upon delithiation [6]. Experimental work by Imanishi et al. showed the reversibility and capacity of Li_2CuO_2 is improved when nickel is substituted for copper, making a Li_2CuO_2–Li_2NiO_2 solid solution [5]. Calculation results indicated that the *Immm* structure might be stabilized by Al and Ga and other transition metal dopants, however an improvement could not be realized experimentally [7].

Lithium removal from copper oxide electrodes upon charging proceeds with irreversible decomposition according to [2,4]

$$Li_2CuO_2 \rightarrow LiCuO_2 + Li^+ + e^- \quad (1)$$

$$2LiCuO_2 \rightarrow 2Li^+ + 2e^- + 2CuO + O_2 \quad (2)$$

* Corresponding author. Fax: +1 202 404 8119.
E-mail address: corey.love@nrl.navy.mil (C.T. Love).

0022-4596/$ - see front matter Published by Elsevier Inc.
doi:10.1016/j.jssc.2011.07.007

The decomposition reaction scheme to produce CuO and oxygen is not complete, possibly by the formation of CuO on the surface of the particles [8]. Prakash et al. has reported that a two-step electrochemical oxidation process is involved in the removal of 1.0 Li^+ from Li_2CuO_2 [3] creating $Li_{1.5}CuO_2$ ($C2/m$) and $LiCuO_2$ ($C2/m$) phases. The $Li_2CuO_2 \leftrightarrow Li_{1.5}CuO_2$ transition had high initial capacity with poor capacity retention while the $Li_{1.5}CuO_2 \leftrightarrow LiCuO_2$ transition had lower initial capacity with good retention. Clearly the structural transformations associated with the $Li_{1.5}CuO_2 \leftrightarrow Li_{2-z}CuO_2$ transition are highly detrimental to electrochemical reversibility in this system [3], whereas $LiCuO_2 \leftrightarrow Li_{1.5}CuO_2$ transformation was found to be highly reversible. The structural stability in the highly lithiated copper oxide system is not fully understood, such as the lack of the reversibility of the *Immm* structure, the packing of the CuO_4 square chains, electron loss from oxygen bands in trivalent copper oxide compounds, high oxidation state of copper, and even the existence of a displacement type reactions.

The fundamental understanding of the instabilities in high capacity Li_2CuO_2 is critical to enabling the design and discovery of future materials. We study the instabilities of Li_xCuO_2 at different states of charge, as obtained by electrochemical delithiation and lithiation during typical battery charging-discharging to formulate a broader understanding of the ties between structural transformation and capacity loss. The resulting Li_xCuO_2 materials are probed with high-energy X-ray diffraction (XRD) and analyzed using the pair-distribution function (PDF) and Rietveld refinement, to resolve the phase composition, and local and medium-range structure from 0.1 to 1.5 nm of the materials' various states of charge (lithiation). This approach provides information about the distribution of interatomic Cu–Cu, Cu–O and O–O distances, and reflects the local changes occurring during charging and discharging. The Li_2CuO_2 *Immm* structure is modeled with density functional theory (DFT) to gain fundamental understanding of the chemistry of this material, and provide insight into material stability.

2. Materials and methods

2.1. Materials preparation

Li_2CuO_2 was prepared by solid-state synthesis. Stoichiometric amounts of $LiOH \cdot H_2O$ (Alfa Aesar, 98%) and CuO (Alfa Aesar, 97%) were ground individually. Once ground, the powders were mixed together, pressed into pellets and calcined in static air at 800 °C for 15 h. A 3% mass excess of $LiOH \cdot H_2O$ was added to account for lithium loss at high temperature. The resulting pellets were ground in mortar and pestle in air and stored in an argon-filled glove box.

2.2. Electrode fabrication and electrochemical testing

Aluminum current collector foils were etched in 1M KOH, rinsed with DI H_2O, and wiped clean with acetone [9]. A slurry of the active material, Li_2CuO_2, was prepared consisting of: 83% Li_2CuO_2, 4% KS-6 graphite, 2% Super P Li-grade carbon, and 4% polyvinylidene fluoride. The PVDF binder was a 5% by weight solution in 1-methyl-2-pyrrolidone (NMP). After thorough mixing, the slurry was applied to the Al-foils and dried at 120 °C under vacuum for at least 12 h. The mass of active material was maintained between 30 and 40 mg Li_2CuO_2 over a 1 in^2 surface area. Negative electrodes were assembled from copper foils etched in 1 M HNO_3, rinsed with DI H_2O, and wiped clean with acetone. The electrodes were introduced into an Ar-filled glove box. A thin layer of lithium metal was rolled onto the copper foil surface in the glove box. The positive and negative electrodes were assembled into a "pouch" cell construction with a Celgard® porous polypropylene membrane. A small amount of 1 M $LiPF_6$ in 1:1 (v:v) ethylene carbonate/diethyl carbonate solvent electrolyte was wet onto the surface of both electrodes before packaging in a tri-foil pouch.

The batteries were charged and discharged using a Maccor 2300 battery tester over a voltage range of 1.5–4.2 V against the lithium metal anode at a $C/25$ rate (~9.8 mA) constant current. Batteries were taken off the charging or discharging cycles at the voltages given in Table 1. The positive electrode mixture Li_xCuO_2+electrode additive (Super P, K-6 graphite, PVDF) was then rinsed with diethyl carbonate to remove residual $LiPF_6$ electrolyte salt and scraped off of the aluminum current collector and dried under vacuum. The cathode mixtures were then heat-sealed in silica tubes before removal from the glove box for ex-situ high-energy XRD analysis.

2.3. Materials characterization

High-energy X-ray diffraction patterns were collected for the cycled Li_xCuO_2 materials at various states of charge (SOC) according to Table 1. Multiple cells were prepared and reproducibility was confirmed. Diffraction patterns were collected for as-prepared Li_2CuO_2 and cycled Li_xCuO_2 materials. Additional baseline measurements were performed on the electrode additives (Super P, K-6 graphite, PVDF) and an empty silica tube. The measurements were done at the 11-ID-C and 6-ID-C beamlines at the Advanced Photon Source (APS) with incident X-ray energy of 115 and 100 keV. The experiment was performed with the image plate detector (MAR-345) placed ~30 cm behind the sample. This setup allows the pair-distribution function analysis and Rietveld refinement to be carried out at the same time. In addition, several samples were measured with the detector ~100 cm behind the sample to carry out high resolution Rietveld. The main advantage of a 2D detector is its ability to cover a large portion of Q-space, thus increasing statistics and decreasing exposure time. Typically we accumulated about 6–8 exposures for each data set. The 2D detector pattern was integrated over the 360° azimuth angle to obtain the intensity as a function of the magnitude of the scattering vector Q. The detector calibration was done using CeO_2 and Si NIST powder standards. FIT2D program [10] was used to correct data for detector geometrical errors due to small angular misalignments, obliqueness, X-ray beam polarization, dark current and incident monitor counts, and for 2D image generation and file format conversion. The silica tube backgrounds were determined separately and subtracted during data analysis.

Table 1
Voltage and cycling parameters for electrochemically delithiated Li_2CuO_2.

Sample	Cut-off voltage		Current (mA)	Cycles #	Capacity (mA h/g)	Notes
	Charge	Discharge				
A	NA	NA	NA	NA	NA	As-prepared electrode
B	4.0	–	9.8	1	229	Charge only
C	4.2	–	9.8	1	255	Charge only
D	4.2	2.0	9.8	1	–	1 full cycle
E	4.2	1.5	9.8	1	–	1 full cycle
F	4.2	1.5	9.8	1+	–	Ending on 4.2 V charge
G	4.2	1.5	49.0	10	–	10 full cycles
H	4.2	1.5	49.0	10+	–	Ending on 4.2 V charge
I	3.3	–	9.8	1	100	Abbreviated charge

Azimuthally integrated intensities were processed using the pdfgetX2 [11] package to obtain the structure function and the reduced pair-distribution function, $G(r)$. $G(r)$ is obtained from the direct Fourier transformation of the total scattering function including Bragg peak and diffuse scattering intensities, as previously described [12] and given in Eq. (3), where scattering vector $Q=4\pi \sin\theta/\lambda$, and θ is the scattering angle and λ denotes wavelength of the probe

$$G(r) = \frac{2}{\pi}\int_0^\infty Q[S(Q)-1]\sin(Qr)\,dQ \quad (3)$$

The diffraction data were analyzed using GSAS [13,14] to verify physical phases and crystallographic structures. The PDF data were fitted to the structures in the real space using *pdfgui* software [15].

2.4. Density functional theory

Density functional calculations were done using the Vienna Ab Initio Simulation (VASP) [16] program within the Projector Augmented Wave PAW formulation [17], using the Generalized Gradient Approximation (GGA) [18] to the exchange correlation potential. Both the lattice parameters and internal coordinates were simultaneously and fully relaxed in the *Immm* and *C*2/*m* structures. Our results were within 1.8% of the experimentally determined structural parameters [5]. To investigate electron withdrawal during charging, the number of electrons in Li_2CuO_2 was decreased by one and a uniform positive background (jellium) was added in order to maintain charge neutrality.

3. Results

The galvanostatic charge/discharge data for Li_2CuO_2 is given in Fig. 1. The features of this curve are representative within several electrode samples and over two batches of material. The long charge plateau near 3.4 V is characteristic of the oxidation of Li_2CuO_2, as reported by Vitins et al. under similar charging conditions [4]. The 256 mA h g^{-1} charge capacity matches the theoretical capacity for removal of 1 Li^+ and the complete conversion of Cu^{2+} to Cu^{3+}. Li_2CuO_2 exhibits poor capacity retention after the initial charge yielding a discharge capacity of 100 mA h g^{-1}, equivalent to only 0.4 mol lithium as also observed by Imanishi et al. [5]. The full capacity of 100 mA h g^{-1} is retained during the second charge cycle inferring any structural changes or reactions occurring after the initial discharge are reversible. However, as will be shown later, subsequent cycles result in a loss of capacity and irreversible structural transformations.

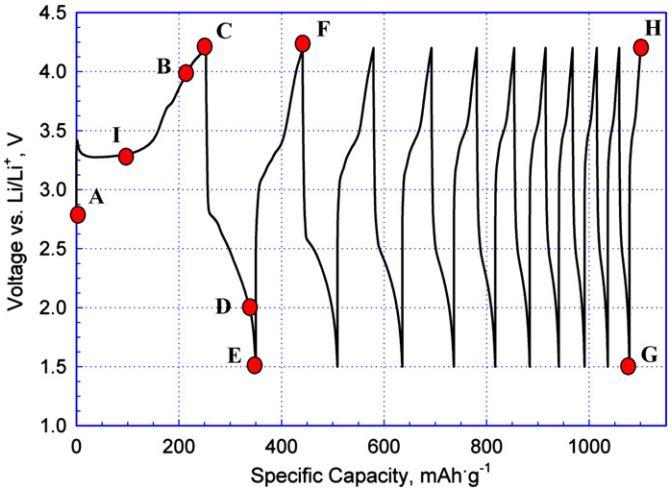

Fig. 1. Constant current charge/discharge of Li_2CuO_2 vs. lithium metal at *C*/25 (~9.8 mA) rate.

Three known phases of Li_xCuO_2 and CuO were identified in the Rietveld refinement of the diffraction patterns of the samples during different stages of the charge and discharge in Fig. 2. Generally, only the as-prepared materials were close to single phase with small contamination. Samples collected during charging and discharging had 3–4 phases of varying ratio. The diffraction pattern for the starting Li_2CuO_2 material, Sample A, can be indexed with the *Immm* orthorhombic space group with $a=3.654$ Å, $b=2.859$ Å, and $c=9.374$ Å. Three-dimensional representations of the *Immm* and *C*2/*m* structures are shown in Fig. 3 for reference. Li occupancy was fixed at 100% for each structure since X-ray data is not sensitive to the content of Li especially in the multiphase samples. Refinement of the oxygen yields values close to the full occupancy of the oxygen-ion sites. There is only one small peak at 2.48 $Å^{-1}$ which is matched to CuO in the Rietveld analysis, which was not fully reacted during synthesis. The integrated intensity of this CuO impurity is low (~1/30) compared to the main phase. However, on a subsequent sample set, the CuO content was found to be 15% of the initial phase (~1/7), possibly the result of CO_2 chemisorption of Li_2CuO_2 [19]. The cumulative effect of a CuO phase with electrochemical cycling is discussed later.

The diffraction pattern for Li_xCuO_2 during initial charge to 4.2 V (Sample C) is also shown in Fig. 2. The pattern can be refined with a majority of the *C*2/*m* layered structure of $LiCuO_2$ which matches the literature [20]. A small fraction of the experimentally observed pattern is the remainder of the unconverted Li_2CuO_2 phase. Generally, the two-phase Rietveld refinement of $LiCuO_2$ at 4.2 V is satisfactory. Sample B at 4.0 V is a mixture of Li_2CuO_2 and $LiCuO_2$ (shown in cumulative summary).

The diffraction patterns for samples discharged to 2.0, 1.5, and 1.5 V after 10 cycles are presented as Sample D, E, and G, respectively, in Fig. 2. The observed intensities are fitted with a mixture of 3–4 phases of Li_2CuO_2, $Li_{1.5}CuO_2$, $LiCuO_2$, and CuO. At deep discharge to 1.5 V, the CuO phase begins to appear in fractions that are beyond the impurity level. This suggests that CuO is the product in some of the lithiation (discharge) reactions. Generally, the observed peaks in Samples D, E, and G are in the correct locations as defined by the calculated structures. However, the intensities do not fit well as indicated by a significant residue; where residue is defined as the difference between the experimentally observed and the calculated theoretical phases. The large residue in the refined intensities clearly suggests structural deviations from the ideal phases. This must be a result of non-ideal Li stoichiometry. The reversibility of lithium reactions are never complete and ideal phases are never recovered. Hindered diffusion of Li results in a range of $Li_{2-x}CuO_2$ phases, concentration gradients and small grain size. Non-ideal stoichiometry, structural distortions, broad, overlapping, and damped peaks make it difficult to understand the structural features that lead to irreversibility and loss of the charging/discharging capabilities from the Rietveld refinement alone. Further structural analysis, through the PDF, is helpful to isolate the structures detrimental to reversible electrochemical cycling.

Fig. 4a presents the experimental pair density function, $G(r)$, for as-prepared Sample A in the Li_2CuO_2 phase, Sample C at 4.2 V, and Samples D and E on discharge. The $G(r)$ of Sample A and C can be fitted well to the respective structures. We can see from this figure that delithiation results in quite significant changes in the pair density function. To understand the meaning of the $G(r)$ peaks and resulting structural changes we have calculated the contribution of different atomic pairs to the $G(r)$. The $G(r)$ is heavily weighted by Cu–B (B=Cu, O, Li) pair correlations. The weighting is

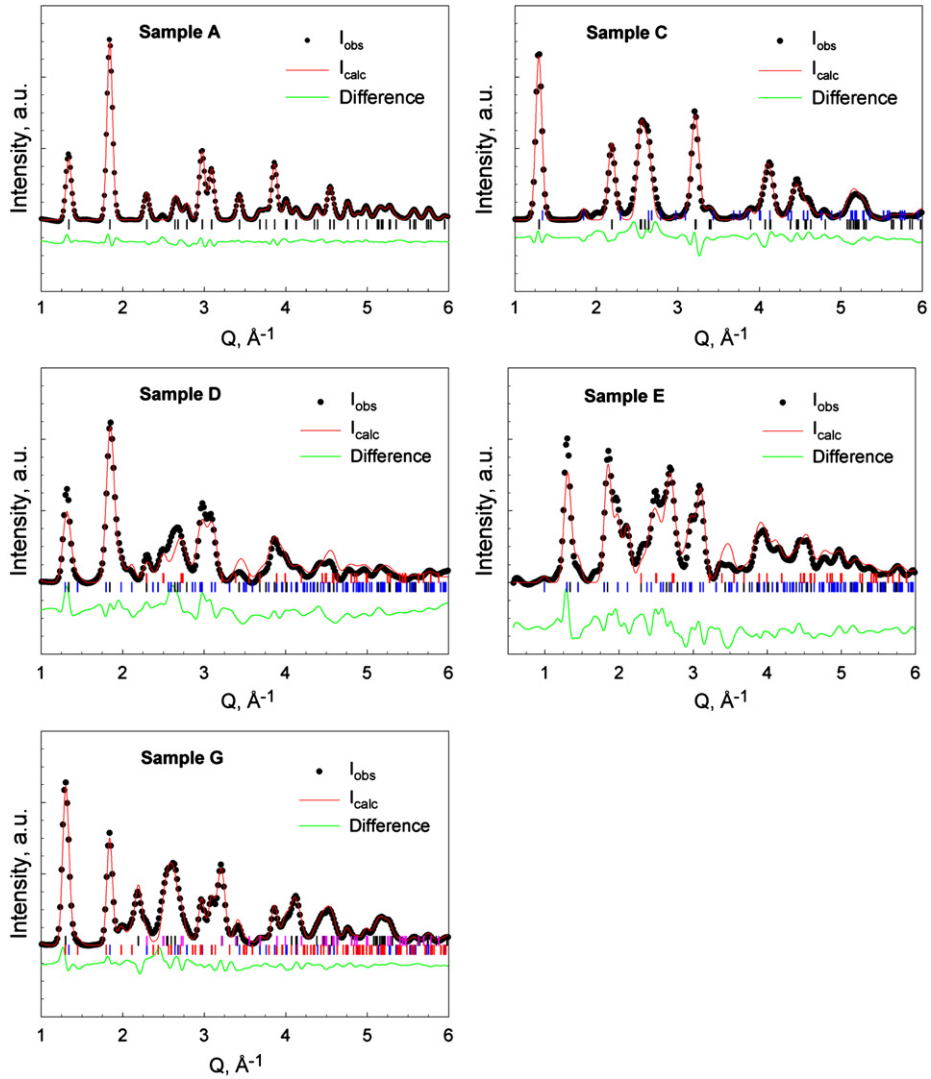

Fig. 2. X-ray diffraction patterns for Li_2CuO_2 Sample A, as-prepared; Sample C, first charge cycle to 4.2 V; Sample D, first discharge cycle to 2.0 V; Sample E first discharge cycle to 1.5 V; Sample G, 10th discharge cycle to 1.5 V. Each plot includes the Rietveld fit. The data are plotted as a function of the scattering vector Q ($Q=2\pi/d$, where d is an inter-planar spacing).

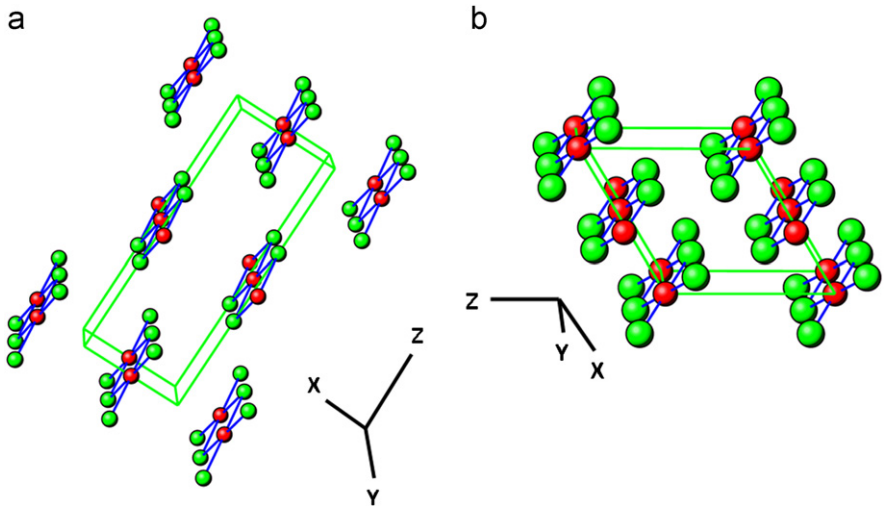

Fig. 3. Three-dimensional representations of (a) *Immm* structure and (b) the *C*2/*m* structure. Copper atoms are represented by red spheres and oxygen green spheres. Lithium atoms have been removed for clarity. (For interpretation of the references to color in this figure legend, the reader is referred to the web version of this article.)

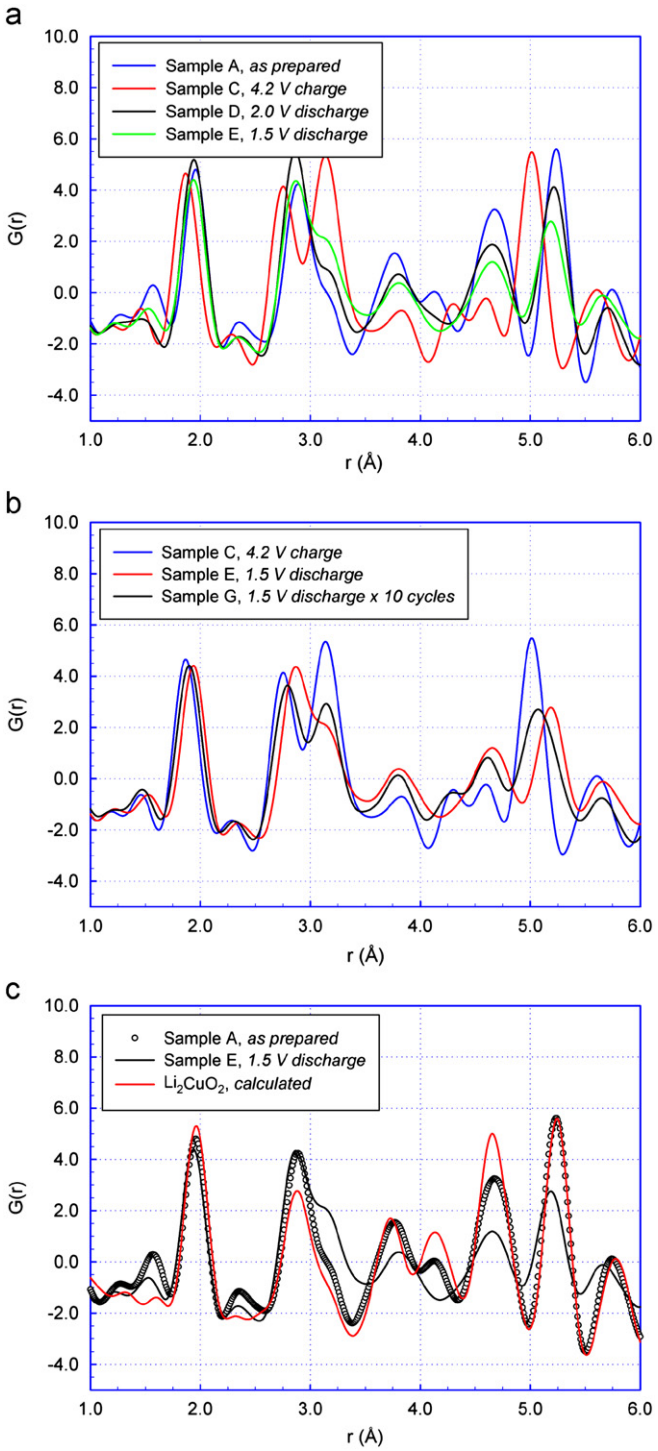

Fig. 4. (a) Atomic pair-distribution function (PDF) illustrating the phase transformations within the initial charge and discharge cycle of Li_2CuO_2 from as-prepared (Sample A); charged to 4.2 V (Sample C); discharged to 2.0 V (Sample D); and fully discharged to 1.5 V (Sample E). (b) The existence of the distorted $LiCuO_2$ phase after complete discharge to 1.5 V (Sample E), and the propagation to a more severely distorted $LiCuO_2$ phase after 10 discharge cycles to 1.5 V (Sample G). The $G(r)$ for the nearly ideal $C2/m$ $LiCuO_2$ phase with slight CuO impurity (Sample C) is given for reference. (c) The incomplete structural transition between as-prepared (Sample A) *Immm* Li_2CuO_2 and fully discharged to 1.5 V (Sample E) with the calculated $G(r)$ for the ideal *Immm* phase given for reference. (For interpretation of the references to color in this figure legend, the reader is referred to the web version of this article.)

proportional to $c_i c_j Z_i Z_j$ (c and Z are atomic concentration and atomic number for element i, j) with Cu having a much larger Z than the other elements. Fig. 5a and b shows the contributions from Cu–Cu, Cu–O, and Cu–Li pairs to the $G(r)$ calculated for the ideal structure for easy identification of the composition and distance of the main peaks in the $G(r)$. The $G(r)$ for Sample A (blue line in Fig. 4a) shows a first major peak at 1.94 Å. This peak corresponds to the Cu–O bonding in the CuO_4 square chains. The observed distance is consistent with the typical ionic radius of the Cu^{2+} in the square coordination as estimated by Shannon [21]. The peak at 2.86 Å represents the Cu–Cu nearest distance. The left and right shoulders of this peak correspond to Cu–Li pairs. The right shoulder is more visible due to the higher number of Li atoms at this distance. The $G(r)$ pattern is dominated by strong peaks due to Cu–Cu pairs at 3.77, 4.67, and 5.22 Å.

The $G(r)$ after charging to 4.2 V (Sample C) is show in red in Fig. 4a. The fit to $G(r)$ (not shown) confirms the phase transformation from the *Immm* structure to the $C2/m$ structure of $LiCuO_2$ as previously discussed in the Rietveld refinement (Fig. 2c). The overall fit of the PDF is in good agreement with the monoclinic structure. The calculated contributions from different atomic pairs are shown in Fig. 5b. The first peak at 1.87 Å in the $G(r)$ indicates the Cu–O distance where the same CuO_4 square chain coordination exists but with a reduction in the ionic radius of copper. The decrease in ionic radius reflects a higher oxidation state of copper upon delithiation as the ionic radius of Cu^{3+} is smaller than Cu^{2+}. The next 2 peaks at 2.75 and 3.14 Å are the result of overlapping Cu–Cu, Cu–O, and Cu–Li pairs. However, the

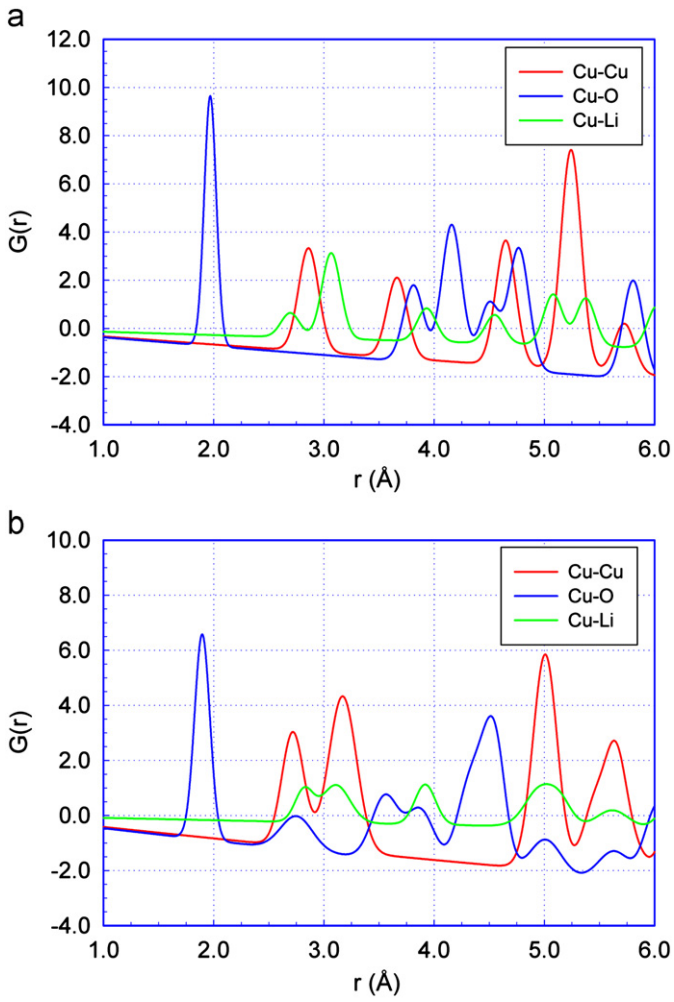

Fig. 5. (a) The partial atomic PDFs for Li_2CuO_2 calculated from the ideal *Immm* structure and (b) the partial atomic PDFs for $LiCuO_2$ calculated from the ideal $C2/m$ structure. (For interpretation of the references to color in this figure legend, the reader is referred to the web version of this article.)

Cu–Cu pairs contribute most of the weight because of their higher Z. The next 3 peaks observed in the experimental $G(r)$ are mostly due to Cu–O distances whereas the large peak at 5.05 Å is again due to Cu–Cu pairs. It is observed from Fig. 5a and b that upon charging (delithiation) there is a significant change in the peaks weighted strongly by Cu–Cu pairs. This is a consequence of denser packing of the CuO_4 square chains in the $C2/m$ structure and overall increase in the physical density.

The PDF data for samples that are discharged to 2.0 and 1.5 V (Samples D and E) are shown in Fig. 4a with black and green lines. Lithiating the structure should initiate the transition from $C2/m$ back to the original *Immm* structure of the Li_2CuO_2. However, it is clear from the PDF data in Fig. 4c the transition is never completed. The as-prepared Li_2CuO_2 (Sample A) is in good agreement with the ideal calculated phase of $G(r)$ considering that Sample A contains electrode diluents such as carbon and polymer binder. The sample discharged to 1.5 V (Sample E) is more disordered with smaller $G(r)$ amplitudes where the shoulder at 3.2 Å is too strong and the peak at 4.2 Å is missing completely. A shift in the first peak towards 1.938 Å As well as higher order peaks are shifted towards smaller r indicate mixed oxidation states of Cu. This was already observed in the Rietveld refinement, which indicated appearance of other phases like $Li_{1.5}CuO_2$ and CuO in addition to the Li_2CuO_2. The $Li_{1.5}CuO_2$ phase is observed near 4.0 V on discharge and is structurally in-between the Li_2CuO_2 (*Immm*) and $LiCuO_2$ ($C2/m$) phases where the packing of the CuO_4 square chains is higher in the $Li_{1.5}CuO_2$ than in the Li_2CuO_2 phase. Clearly from the electrochemical data in Fig. 1, discharge to 2.0 V does not fully re-intercalate lithium and leads to the loss of capacity. Surprisingly, further depth of discharge to 1.5 V is not useful for re-intercalation either. Instead of complete lithiation to Li_2CuO_2, discharging to 1.5 V actually reduces the likelihood of achieving the fully lithiated Li_2CuO_2 phase. The $G(r)$ of the 1.5 V discharged sample is shown in Fig. 5a (green line). We expect the peaks in the $G(r)$ at 5.2 or 4.6 Å would be closer to the Li_2CuO_2 phase (blue line) than Sample D, discharged to 2.0 V (black line); however, this is not observed here. The peaks are lower in intensity and slightly shifted compared to the Li_2CuO_2 as-prepared material. Similarly, the opposite changes are observed in the 3 Å range. This may be related to the formation of CuO as detected by Rietveld. Further evidence of unusual structural changes at deep discharges are shown in Fig. 4b. The $G(r)$ of the Sample G, which has been discharged 10 times to 1.5 V (black line), is shown together with Samples E and C. Unexpectedly, multiple discharge cycles drive the local structure closer to the PDF characteristic of $LiCuO_2$. The formation of CuO should be accompanied by oxygen release. PDF results show the highly ordered loose packing of the CuO_4 square chains in the *Immm* structure are never recovered after discharge. The Cu–Cu peaks in the $G(r)$ of the discharged samples are lower in magnitude (therefore broader) and shifted in position indicating non-homogeneous distribution of the square chains. To achieve the fully discharged state the structure has to expand to accommodate lithium. However, re-intercalation of lithium is partially blocked by the structural changes. The Cu atoms maintain the square coordination however; it is the changes in the packing of the chains that is responsible for reduced Li intercalation. After multiple discharge cycles to 1.5 V no further reduction of CuO to Cu_2O is observed. The electrochemical reduction to Cu+ has been observed previously by Debart et al. within the 1.6–1.3 V range [22].

The release of oxygen from delithiated cathode materials promotes structural instability leading to decreased capacity retention. Density functional theory was applied to investigate the electronic structure of Li_xCuO_2 as a function of x, with the possibility of oxygen loss in mind. Fig. 6a shows the density of states (DOS) of Li_2CuO_2. The top of the valence band, from which electrons are withdrawn during delithiation, is clearly composed of an equal mixture of Cu and O, indicating that both Cu and O will be oxidized during charging. Therefore, a simple picture in which Cu changes from 2+ to 3+ is inapplicable to this material. In fact, an analysis of the partial charge densities shows that 30% of the lost charge comes from the Cu ion, and 35% from each of the two O ions in the unit cell. Since it is well known that DFT consistently overestimates the energy position of transition metal d-states, the Cu-derived DOS should almost certainly be pushed even lower in energy and consequently, the proportion of O at the Fermi energy is likely to be even higher than calculated. A more intuitive illustration of charge loss can be seen in Fig. 6b, calculated from the subtraction of the electron density of Li_2CuO_2 from the electron density of Li_2CuO_2 less $1e^-$ (the Li^+ remains in the system to highlight the electronic, as compared to ionic, subsystem). The yellow "clouds" show where electron density has been lost during the charge; green areas show where electron density has been gained. As expected, there is electron loss around Cu, but the equal (slightly greater) amount lost from

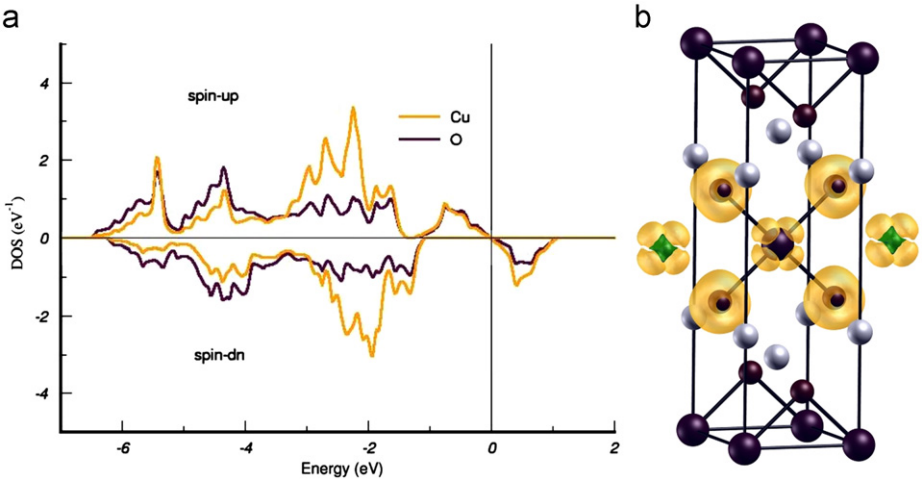

Fig. 6. (a) Density of States plot for Cu and O in Li_2CuO_2 in the *Immm* structure and (b) charge density of Li_2CuO_2 when an electron is removed from the structure. The yellow clouds indicate lower density while the green indicate where there is more charge being removed. (For interpretation of the references to color in this figure legend, the reader is referred to the web version of this article.)

O sites is also clear. This charge removal shifts the oxygen ion away from its preferred 2-valence, making it susceptible to release from the structure as gas or to transformation to more stable compounds such as CuO. Calculations also show that Li_xCuO_2 is most stable in the *Immm* structure at $x=2$, but that *C*2/*m* is the lowest energy state at $x=1$. As PDF data show, part of the material does return to the lower energy *Immm* symmetry upon re-lithiation, but with significant local disorder. Calculations indicate that this may be partially attributable to permanent oxygen loss incurred during the charging part of the cycle.

4. Discussion

The lack of copper metal (Cu^0) and Li_2O in the refined Rietveld and PDF analysis suggest the irreversible reactions within the highly lithiated copper oxide materials is not due to displacement type reactions. The contributing Li–Cu–O phases observed through Rietveld and PDF analysis is illustrated in Fig. 7 with the phase content of various charge/discharge conditions. The phase content is corrected to assume 100% pure Li_2CuO_2 starting material in Sample A. During an abbreviated initial charge to 100 mA h g^{-1} (Sample I), two phases are present, the Li_2CuO_2 starting material and the delithiated phase, $LiCuO_2$. A full Li^+ is removed at 245 mA h g^{-1} as indicated by the dominate $LiCuO_2$ phase (Sample C). A small fraction of a new phase, CuO, is observed at 245 mA h g^{-1} for starting material with an initial CuO impurity. With repeated cycling of the contaminated materials, the *C*2/*m* phase is suppressed with the growth of the CuO phase. This suggests a non-uniform removal of lithium, where the sum of lithium ions removed is 1 at 4.2 V; however, two reaction mechanisms contribute to donate 1 Li^+:

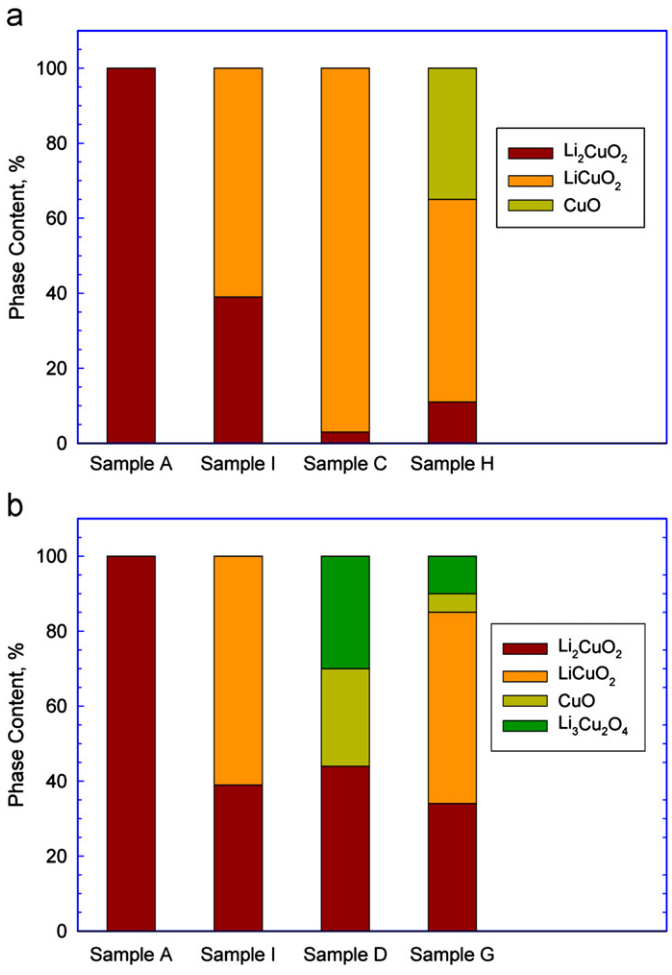

Fig. 7. (a) Phase content during charging to 4.2 V on the initial charge (Sample C) and after 10 charge cycles (Sample H) with the as-prepared Li_2CuO_2 (Sample A) and during the initial charge to 100 mA h g^{-1} (Sample I) given for reference; (b) phase content after discharge to 2.0 V on the initial discharge (Sample D) and after repeated cycling to 1.5 V (Sample G) with the as-prepared Li_2CuO_2 (Sample A) and during the initial charge to 100 mA h g^{-1} (Sample I) given for reference.

$$Li_2CuO_2 \rightarrow Li_{2-x}CuO_2 + xLi^+ + xe^- \quad (4)$$

$$Li_{2-x-y}CuO_2 \leftrightarrow CuO + yLi^+ + 1/2O_2 \ (x+y \approx 1) \quad (5)$$

Where $Li_{2-x-y}CuO_2$ in *C*2/*m* structure contains local atomic distortions but still provides 1 Li^+ (245 mA h g^{-1}).

A mixed Li_2CuO_2–$LiCuO_2$ phase appears during the initial discharge plateau near 2.6 V suggesting some degree of reversibility during the removal and introduction of 1 Li^+ to and from the *Immm* structure. However, this is not a completely reversible reaction leading to the decomposition of the delithiated $LiCuO_2$ *C*2/*m* phase as in Eq. (4). The presence of the CuO phase is observed at 2.0 V (Sample D) where CuO has initiated due to the incomplete lithiation of Eq. (5). The lithiation of the *C*2/*m* structure to the *Immm* requires a large structural change as shown in the pair-distribution function in Figs. 4 and 5, and is accompanied with a significant variation in density from 3.7 g cm^{-3} for Li_2CuO_2 to 4.5 g cm^{-3} for $LiCuO_2$ [2]. The corrugated copper square chains prevent transformation to the orthorhombic structure and reduce the lithium capacity of the material. On discharge, the following reactions are likely:

$$Li_{2-x-y}CuO_2 + Li^+ + e^- \rightarrow Li_2CuO_2 \quad (6)$$

$$CuO + xLi^+ + zO_2 \rightarrow Li_xCuO_y \quad (7)$$

where partially lithiated Li_xCuO_2 can take on the $LiCuO_2$ and $Li_3Cu_2O_4$ phases. The secondary reactions of Eqs. (5) and (7) require small structural changes; however rely on the presence of structural oxygen. However, lithium insertion into $LiCuO_2$ has previously been shown to cause a loss of crystallinity by Arai et al. [2]. A decrease in Li_2CuO_2 crystallinity is also observed in this work, as evidenced by the diffuse diffraction pattern and confirmed by the broad and damped PDF peaks. The existence of an intermediate phase, $Li_3Cu_2O_4$, solved by Currie [8] was observed here with careful analysis of the Rietveld refinement. This was not observed using powder diffraction alone in another work [4]. The most intriguing result is the inverted phase content after multiple cycles. Fig. 7 shows that after 10 cycles $LiCuO_2$ is present at the discharged state (Sample G). Ideally this condition should not contain $LiCuO_2$ but should revert back to the original Li_2CuO_2 phase. The tendency towards structures close to $LiCuO_2$ after multiple discharges is confirmed by inspecting the first Cu–O peaks in the $G(r)$ (Fig. 8). The Cu–O distance is decreasing with multiple discharges; thus significant fraction of copper must exist in the 3+ state as evident by the shorter average bond length. The Cu–O distance in the CuO phase is the same as in Li_2CuO_2 as expected for Cu^{2+}. Also unexpectedly CuO accumulates in the discharged state after many cycles as seen in Fig. 7. CuO is most likely formed through the delithiation reaction in Eq. (7) on charging. This is possible because there are Li concentration gradients and at the end of the discharge cycle there is also significant amount of the $LiCuO_2$ phase present. The precipitation of CuO strongly affects reversibility (as in Eq. (1)) and can lead to the reactions in Eqs. (5) and (7) contributing to the capacity loss mechanism over multiple cycles. The structural disorganization and loss of reversibility in the electrochemically cycled Li_2CuO_2 system is not the result of the change in CuO_4 coordination itself, or Cu atoms substituting Li sites but rather the effect of packing of

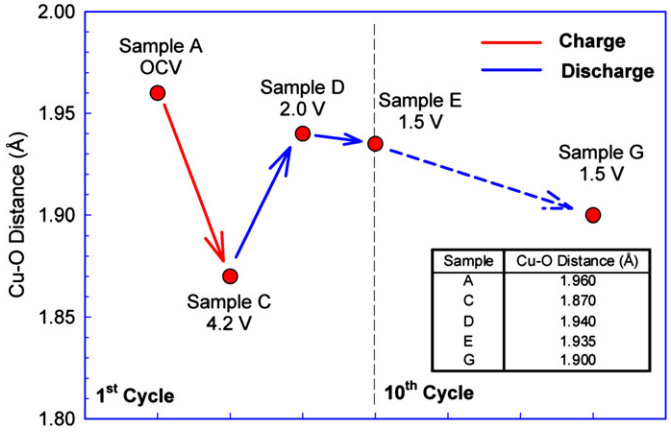

Fig. 8. Schematic mapping of first Cu–O peak distance in the $G(r)$ analysis for Li_xCuO_2 charged and discharged to various states of charge.

the square chains. This is why there is some reversibility between $Li_{1.5}$ and $Li_{1.0}$ where the both phases maintain the $C2/m$ structure with similar packing density of the CuO_4 square chains.

5. Conclusions

Li_2CuO_2 is an attractive cathode material for lithium-ion battery applications due to its high initial charge capacity over 250 mA h g^{-1} in a relatively low-cost (compared to cobalt systems) and non-toxic material. However, only one third of the charge capacity is retained during discharge. We used electrochemistry, high-energy X-ray diffraction with pair-distribution function analysis, and density functional theory to study the instabilities of this highly lithiated copper oxide material at varying state of charge to formulate a broader understanding of the ties between structural transformation and capacity loss. We found that after initial charge a multiphase material persisted through the charge–discharge cycle. Reversibility was not obtained even at deep discharge and after many cycles. We observed the formation of CuO, which accumulated in the charged state suggesting that CuO can be a product of the delithiation reaction which must be accompanied by oxygen release. Surprisingly, $LiCuO_2$ was observed in the discharged state. The precipitation of CuO strongly affects the reversibility of the lithiation reactions contributing to capacity loss. The structural disorganization and loss of reversibility in the electrochemically cycled Li_2CuO_2 system is the result of packing of the Cu–O square chains. DFT calculations showed electron removal from both Cu and O during delithiation of Li_2CuO_2. Charge removal from oxygen makes the compound susceptible to the release of oxygen as gas or the formation or more stable compounds such as CuO.

Acknowledgments

The authors are grateful to the Office of Naval Research for support of this work. We would like to thank D. Robinson (APS, 6-ID) and Y. Ren (APS,11-ID) for the help with experimental setup. Use of the Advanced Photon Source is supported by the U.S. Department of Energy (DOE), Office of Science, under Contract No. DE-AC02-06CH11357.

References

[1] E.A. Raekelboom, A.L. Hector, M.T. Weller, J.R. Owen, Journal of Power Sources 97-8 (2001) 465–468.
[2] H. Arai, S. Okada, Y. Sakurai, J.-i. Yamaki, Solid State Ionics 106 (1998) 45–53.
[3] A.S. Prakash, D. Larcher, M. Morcrette, M.S. Hegde, J.-B. Leriche, C. Masquelier, Chemistry of Materials 17 (2005) 4406–4415.
[4] G. Vitins, E.A. Raekelboom, M.T. Weller, J.R. Owen, Journal of Power Sources Selected Papers Presented at the 11th International Meeting on Lithium Batteries 119–121 (2003) 938–942.
[5] N. Imanishi, K. Shizuka, T. Ikenishi, T. Matsumura, A. Hirano, Y. Takeda, Solid State Ionics 177 (2006) 1341–1346.
[6] K. Kang, C.H. Chen, B.J. Hwang, G. Ceder, Chemistry of Materials 16 (2004) 2685–2690.
[7] C.T. Love, M.D. Johannes, A.M. Stux, K. Swider-Lyons, ECS Transactions 16 (2009) 27–35.
[8] D.B. Currie, M.T. Weller, Journal of Materials Chemistry 3 (1993) 229–232.
[9] A.M. Stux, K.E. Swider-Lyons, Journal of the Electrochemical Society 152 (2005) A2009–A2016.
[10] A.P. Hammersley, S.O. Svensson, A. Thompson, Nuclear Instruments & Methods in Physics Research Section A—Accelerators, Spectrometers, Detectors, and Associated Equipment 346 (1994) 312–321.
[11] X.Y. Qiu, E.S. Bozin, P. Juhas, T. Proffen, S.J.L. Billinge, Journal of Applied Crystallography 37 (2004) 110–116.
[12] W. Dmowski, T. Egami, K.E. Swider-Lyons, C.T. Love, D.R. Rolison, Journal of Physical Chemistry B 106 (2002) 12677–12683.
[13] A.C. Larson, R.B. Von Dreele, Los Alamos National Laboratory, 2000.
[14] B.H. Toby, Journal of Applied Crystallography 34 (2001) 210–213.
[15] C.L. Farrow, P. Judas, J.W. Liu, D. Bryndin, E.S. Bozin, J. Bloch, T. Proffen, S.J.L. Billinge, Journal of Physics: Condensed Matter 19 (2007) 335219.
[16] G. Kresse, J. Hafner, Physical Review B 47 (1993) 558–561.
[17] P.E. Blochl, Physical Review B 50 (1994) 17953–17979.
[18] J.P. Perdew, K. Burke, M. Ernzerhof, Physical Review Letters 77 (1996) 3865–3868.
[19] L.M. Palacios-Romero, E. Lima, H. Pfeiffer, Journal of Physical Chemistry A 113 (2009) 193–198.
[20] R. Berger, L.E. Tergenius, Journal of Alloys and Compounds 203 (1994) 203–207.
[21] R.D. Shannon, C.T. Prewitt, Acta Crystallographica Section B—Structural Crystallography and Crystal Chemistry B 25 (1969) 925.
[22] A. Debart, L. Dupont, P. Poizot, J.B. Leriche, J.M. Tarascon, Journal of the Electrochemical Society 148 (2001) A1266–A1274.